Eur J Echocardiography (2000) **1,** 154–170
doi:10.1053/euje.2000.0031, available online at http://www.idealibrary.com on IDEAL®

REVIEW ARTICLE

Regional Strain and Strain Rate Measurements by Cardiac Ultrasound: Principles, Implementation and Limitations

J. D'hooge[1]*, A. Heimdal[2], F. Jamal[3], T. Kukulski[3], B. Bijnens[3], F. Rademakers[3], L. Hatle[3], P. Suetens[1] and G. R. Sutherland[3]

[1]*Medical Image Computing, Department of Electrical Engineering, Katholieke Universiteit Leuven, Leuven, Belgium,* [2]*GE Vingmed Ultrasound, Horten, Norway and* [3]*Department of Cardiology, Katholieke Universiteit, Leuven, Leuven, Belgium*

The non-invasive quantification of regional myocardial function is an important goal in clinical cardiology. Myocardial thickening/thinning indices is one method of attempting to define regional myocardial function. A new ultrasonic method of quantifying regional deformation has been introduced based on the principles of 'strain' and 'strain rate' imaging. These new imaging modes introduce concepts derived from mechanical engineering which most echocardiographers are not familiar with. In order to maximally exploit these new techniques, an understanding of what they measure is indispensable. This paper will define each of these modalities in terms of physical principles and will give an introduction to the principles of data acquisition and processing required to implement ultrasonic strain and strain rate imaging. In addition, the current status of development of the technique and its limitations will be discussed, together with examples of potential clinical applications.

(Eur J Echocardiography 2000; 1: 154–170)

Key Words: Strain; strain rate; ultrasound; myocardium; review.

Introduction

That regional endocardial motion can be used to attempt to define regional myocardial function is a long-standing concept. This tenent has formed the basis of many angiographic, nuclear and two-dimensional (2D) echocardiographic studies[1–4]. A better description of regional myocardial function seems to be given by determining local wall thickening and thinning characteristics, which are not necessarily directly related to endocardial motion. The optimal data set with which to attempt to describe regional myocardial function would define wall deformation characteristics in three dimensions and in real time. Currently, three-dimensional (3D) local wall deformation can be acquired by magnetic resonance imaging[5,6], while computed tomography and gated single-photon emission computed tomography/positron emission tomography (SPECT/PET) imaging enable 3D acquisition of wall thickening and thinning[7,8]. However, none of these are real-time techniques and the current temporal resolution used in clinical practice does not resolve all myocardial mechanical events. In contrast, real-time acquisition of resolved local thickening/thinning parameters can be obtained from ultrasound by grey-scale M-mode recordings, but only in one dimension and for a limited number of regions of the myocardium[9].

Colour Doppler myocardial imaging is a new cardiac ultrasound technique which, in its current high frame rate format (>120 frames . s^{-1}) can resolve all mean

Address for correspondence: Jan D'hooge, University Hospital Gasthuisberg, Department of Cardiology, Herestraat 49, B-3000 Leuven, Belgium.

1525-2167/00/030154+17 $35.00/0

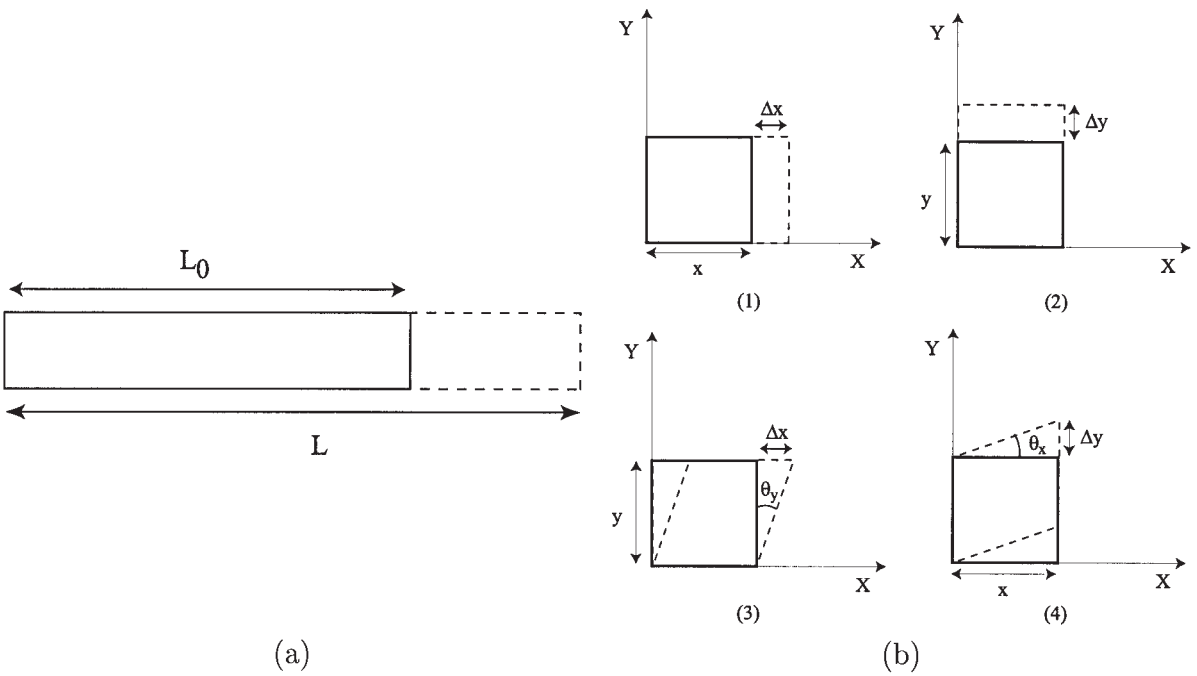

Figure 1. (a) Deformation (strain) of a one-dimensional object is limited to lengthening or shortening. Strain is the deformation of an object relative to its original shape. For a 2D object, deformation, i.e. strain, can be described by four strain components: two normal strains [(b1) and (b2)] and two shear strain components [(b3) and (b4)]. The shear strains are also completely characterized by the angles θ_x and θ_y.

myocardial velocities along its image lines[10,11]. Initial clinical studies have examined the potential diagnostic role of this technique in determining regional myocardial function from velocity data sets for a number of disease entities[12–17]. Although encouraging data were obtained, it was clear that the interrogation of regional myocardial velocities alone has two major drawbacks. Firstly, since the amplitude of the estimated velocity is dependent on the angle at which the region is imaged, accurate quantification of peak velocities can be difficult. Secondly, overall heart motion, rotation and contraction of adjacent myocardial segments will influence regional velocity estimates[18]. In order to overcome some of these problems, ultrasonic strain rate imaging, or in other words, rate of deformation imaging, has been developed by estimating spatial gradients in myocardial velocities. From strain rate curves, local strain (i.e. regional deformation curves) can be extracted, resulting in the concept of regional strain imaging.

These new techniques of regional strain rate and strain imaging introduce concepts derived from mechanical engineering which most echocardiographers are not familiar with. The purpose of this paper is to give an introduction to the physical concepts underlying strain (rate) imaging.

Definitions

Strain

Strain is defined as the deformation of an object, normalized to its original shape. In a one-dimensional (1D) object (i.e. an infinitesimally thin bar), the only possible deformation of the object is lengthening or shortening. This is illustrated in Figure 1(a). The relative amount of deformation is defined as strain. Strain, for which the symbol ε is used, can thus be written as:

$$\varepsilon = \frac{L - L_0}{L_0}, \tag{1}$$

with L the length of the object after deformation and L_0 its original length. Since it is the change in length *relative* to its initial length, it is a dimensionless quantity (often expressed in percent). By convention, equation (1) is defined in such a way that lengthening is represented as a positive value for strain, while shortening is represented by a negative value.

When the length of the object is not only known before and after deformation but also *during* the deformation process, the *instantaneous* strain can be defined:

$$\varepsilon(t) = \frac{L(t) - L(t_0)}{L(t_0)}, \tag{2}$$

with $L(t)$ the length of the object at time instance t and $L(t_0) \equiv L_0$ its initial length. In other words, the instantaneous deformation is expressed relative to the initial length; this is the *Lagrangian strain*. However, the deformation can also be expressed relative to the length at a previous time instance:

$$d\varepsilon_N(t)=\frac{L(t+dt)-L(t)}{L(t)} \tag{3}$$

with dt an infinitesimally small time interval and $d\varepsilon_N(t)$ the infinitesimally amount of deformation occurring during this time interval. The total amount of strain can then be obtained by adding all these infinitesimal strain contributions together:

$$\varepsilon_N(t)=\int_{t_0}^{t} d\varepsilon_N(t). \tag{4}$$

In other words, in this definition of instantaneous strain, the reference value is not constant over time but changes during the deformation process; it is called the *natural strain*. It can be shown that the Lagrangian strain ε and the natural strain ε_N have a fixed (non-linear) relationship which is given by[19]:

$$\varepsilon_N(t)=\ln(1+\varepsilon(t)) \quad \text{or} \quad \varepsilon(t)=\exp(\varepsilon_N(t))-1, \tag{5}$$

where 'ln' is the natural logarithm. Note that this relationship only holds when the rate of deformation is constant as a function of time. If the strains are small (of the order 5–10%) Lagrangian and natural strain values are approximately equal. However, for the large deformations which can occur during cardiac ejection and rapid filling, the difference becomes significant. For this reason it is important to define which type of strain is measured when studying the heart. For cardiac applications, it has been suggested that it may be more appropriate to measure the natural strain, since in that case the measured values are less dependent on the definition of the initial length L_0[19,20].

Until now, the assumption was made that the deforming object was one-dimensional. However, for a 2D object, the deformation is not limited to lengthening or shortening in one direction: it can lengthen or shorten along the x- or y-axes [compare Fig. 1(b1) and (b2)] and can distort by the relative displacement of the upper to the lower border [compare Fig. 1(b3)] or the right border to the left border [compare Fig. 1(b4)]. The first type of deformation [Fig. 1(b1) and (b2)] is referred to as *normal strain* (since its associated motion is normal to the border of the object), while the latter deformation [Fig. 1(b3) and (b4)] is called *shear strain* (since its associated motion is parallel to the border of the object). In order to describe the deformation of a 2D object completely, all four strain *components* have to be known. Mathematically, these components are recognized by their index:

$$\begin{cases} \varepsilon_x=\dfrac{\Delta x}{x} \quad \text{and} \quad \varepsilon_y=\dfrac{\Delta y}{y} \\ \varepsilon_{xy}=\dfrac{\Delta x}{y} \quad \text{and} \quad \varepsilon_{yx}=\dfrac{\Delta y}{x}. \end{cases} \tag{6}$$

It is mathematically convenient to write all strain components in a single matrix as:

$$\begin{pmatrix} \varepsilon_x & \varepsilon_{xy} \\ \varepsilon_{yx} & \varepsilon_y \end{pmatrix} \tag{7}$$

This matrix is refered to as the *strain tensor**. The shear strain components can also uniquely be determined by the angles θ_x and θ_y since their tangent is equal to $\Delta y/x$ and $\Delta x/y$ respectively. Thus:

$$\varepsilon_{xy}=\tan\theta_y \quad \text{and} \quad \varepsilon_{yx}=\tan\theta_x. \tag{8}$$

As in the 1D situation, the *instantaneous strain* components can be defined if the deformation process is known as a function of time. Again, both Lagrangian and natural strain components can be calculated.

The most general situation is that of a 3D object which deforms (as in a myocardial segment). In this case, there are three normal strains (along the x, y and z-axes) and six shear strains (xy, xz, yz, yx, zx and zy). Some of these strain components are illustrated in Figure 2. Defining these nine strain components defines the deformation of the 3D object completely.†

Strain Rate

Strain rate is the speed at which deformation (i.e. strain) occurs. It is represented by the symbol $\dot{\varepsilon}$‡ and has the unit s^{-1}. Although s^{-1} is in fact the same as Hz, it is preferable to use s^{-1} since Hz is normally used to express a periodic change. Clearly, in the most general situation, strain (and thus strain rate) does not necessarily have a cyclic nature, as one can only deform an object once.

For example, if we assume 20% total (Lagrangian) strain of a 1D object (e.g. the object lengthens from its original length of 2 cm to 2.4 cm) and if the total deformation takes 2 s, the average *strain rate* $\dot{\varepsilon}$ is equal to 0·20/2 s, which is 0·1 s^{-1}: on average, the object lengthens by 10% every second. When the same amount of deformation occurs in only half this time period (in this example: 1 s), the average strain rate doubles to 0·20/1 s = 0·2 s^{-1}: on average, the object lengthens by 20% every second. From this example, it is clear that strain rate and strain relate as velocity and distance. For example, when a car drives a particular distance (strain)

*Note that in the mechanics literature the shear strain is often defined as: $\varepsilon_{xy}=\frac{1}{2}(\Delta x/y+\Delta y/x)$. This implies that both shear strain components are identical, i.e. that $\varepsilon_{xy}=\varepsilon_{yx}$. This reduces the number of independent strain components to three, which simplifies stress-strain analysis. However, it is only appropriate for homogeneous, isotropic and incompressible media.

†As in the 2D case, defining the shear strain components as in footnote* reduces the number of strain components to six. Again, this is only appropriate for homogeneous, isotropic and incompressible media.

‡Note that some authors have used the symbol ε' to represent strain rate.

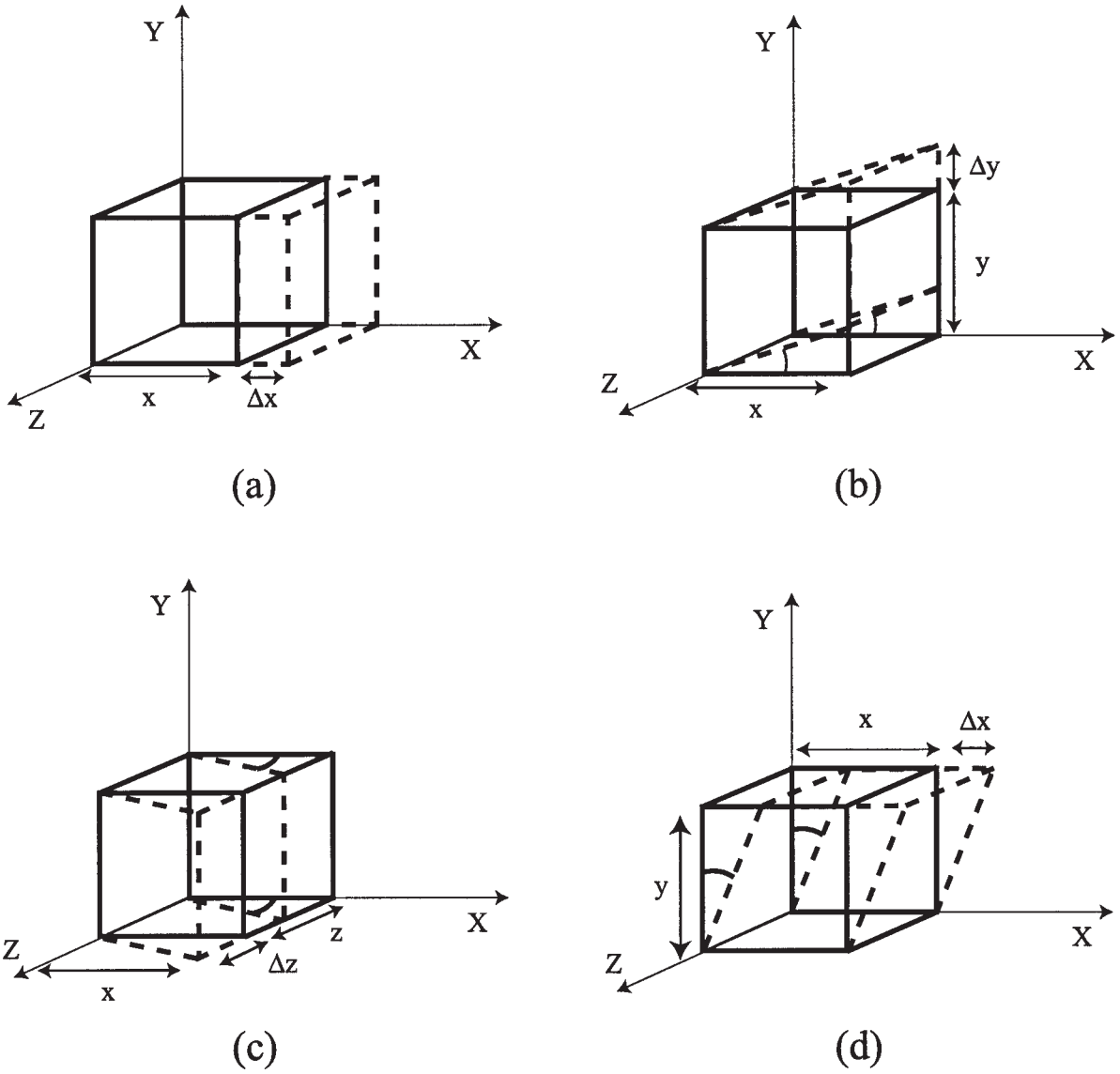

Figure 2. Deformation of a 3D object is described by three normal and six shear strain components. One normal component (a) and three shear components [ε_{yx} (b), ε_{zx} (c) and ε_{xy} (d)] are illustrated here.

in a certain amount of time, the average velocity (strain rate) of the car can be calculated. Note that this does not imply that the instantaneous velocity of the car is known over the whole journey. Similarly, this does not imply that the instantaneous strain rate is known.

Since a 3D object has nine strain components all occurring at a specific rate, nine strain rates can be defined. Since both natural and Lagrangian strain can be defined, both natural and Lagrangian strain rates can be calculated. For the 2-second deformation in the previous example, the natural strain value at the end of deformation is 18·2% [using equation (5)]. This implies an average natural strain rate of 0·0912 s^{-1}. However, since the reference value to calculate the natural strain is not constant over time, the natural strain rate (in this example) is a function of time as well. The instantaneous natural strain rate can be calculated as:

$$\dot{\varepsilon}_N(t)=\frac{L'(t)}{L(t)}, \tag{9}$$

with $L'(t)$ the rate of deformation (e.g. 2·4 cm − 2 cm)/2 s = 0·2 cm . s^{-1}) and $L(t)$ the instantaneous length of the object. This means that in this example the instantaneous natural strain rate drops from 0·1 s^{-1} at the onset of deformation to 0·0833 s^{-1} at the end of the deformation. Note the difference between deformation rate (expressed in m . s^{-1}) and strain rate (expressed in s^{-1}).

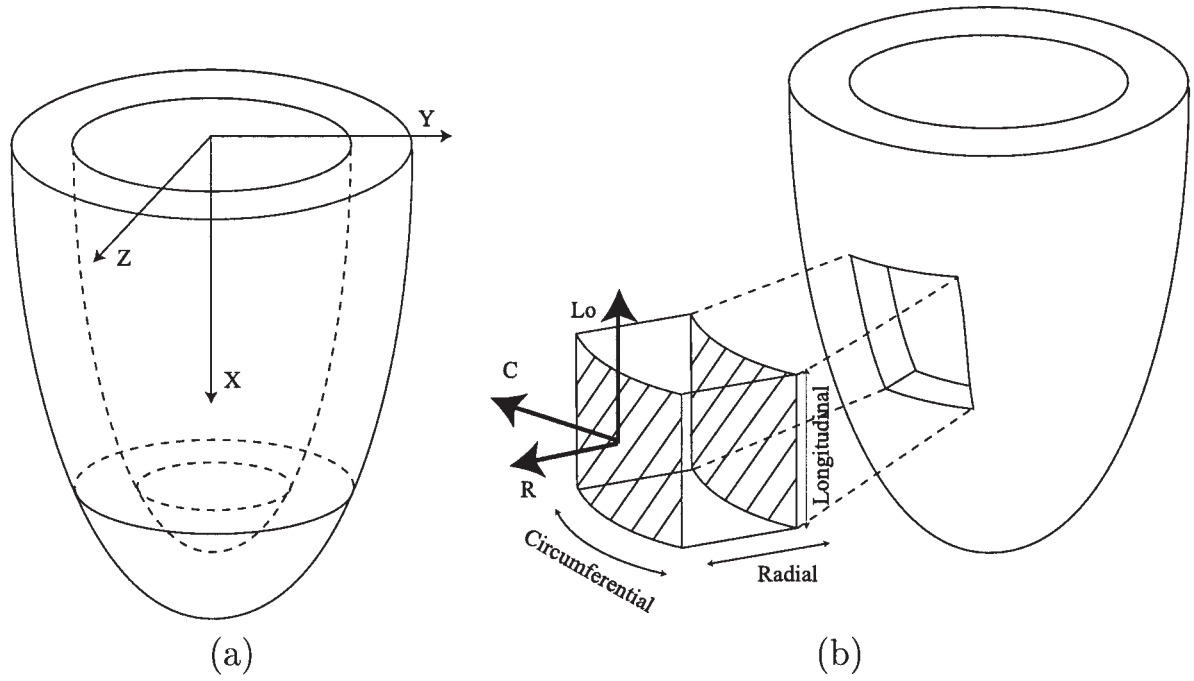

Figure 3. Either a global Cartesian coordinate system (a) or a local heart coordinate system (b) can be defined. However, the latter coordinate system facilitates the physical interpretation of strain measurements of the heart.

The Relationship Between Strain and Wall Thickening

For the heart, wall thickening (WT) is defined as:

$$WT = \frac{T_{ES} - T_{ED}}{T_{ED}}, \tag{10}$$

with T_{ES} and T_{ED} end-systolic and end-diastolic wall thickness, respectively. This expression is clearly identical to equation (1). In other words, wall thickening is nothing but myocardial strain measured in one dimension. Since it compares the end-systolic wall thickness relative to the (fixed) end-diastolic wall thickness, the classical wall thickening parameter in fact measures Lagrangian strain. Clearly, the rate at which the myocardial wall thickens and thins is thus nothing but the 1D strain rate.

Coordinate Systems

In order to uniquely define different positions in space, a 3D coordinate system must be constructed. This is defined to be a set of three different, mutually non-coplanar unit vectors having the same origin. The position of any point within the concomitant 3D space can be expressed relative to these unit vectors. In this way, every single spatial point within the coordinate system can be ascribed a unique coordinate. However, the coordinates of each point will depend on the coordinate system chosen.

Similarly, the strain component measured will depend on the coordinate system used. Using the most appropriate coordinate system is important, as this will facilitate interpretation of the measurements and will reduce the mathematical complexity required to describe the deformation. The possible coordinate systems which can be used in ultrasonic cardiac strain imaging are as follows.

The Heart Coordinate System

Rather than defining a global Cartesian coordinate system in which the whole heart or the left ventricle is described [Fig. 3(a)], a local heart coordinate system can be defined. For each point to be interrogated in any myocardial wall, three mutually perpendicular axes can be defined:

- **The radial (R) axis:** perpendicular to the epicardium, pointing outwards, that is, away from the cavity.
- **The longitudinal (Lo) axis:** perpendicular to the radial axis, that is, tangent to the epicardium, and pointing towards the base of the ventricle, away from the apex.
- **The circumferential (C) axis:** perpendicular to both the radial and longitudinal axis, defined in such a way that the R–Lo–C coordinate system is right-handed (if one looks along the C-axis, the rotation from the R to the Lo-axis is clockwise). Thus, the circumferential axis is directed anticlockwise around the classical echo short axis image.

This local coordinate system is illustrated in Fig. 3(b). Note that the spatial orientation of the three local axes

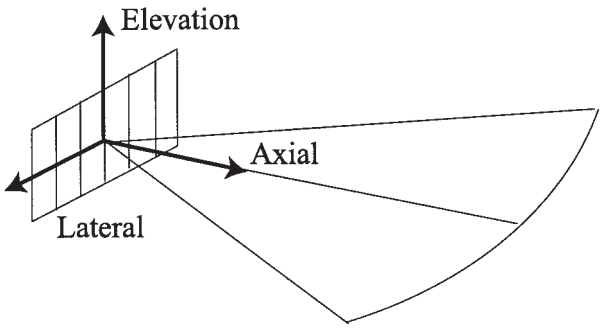

Figure 4. The ultrasound coordinate system has axial, lateral and elevation axes which are, respectively, along the image line, perpendicular to image line and within the image plane and perpendicular to the image plane.

relative to the global coordinate system is different for each point within the ventricle. Moreover, note that this coordinate system cannot be defined for the most distal point of the apex of the ventricle, as here neither a circumferential direction nor a longitudinal orientation can be defined.

The Ultrasound Coordinate System

Within an ultrasound image, an ultrasound coordinate system can be defined, with its centre at the position of the transducer, by the following three axes:

- **The axial (A) axis:** along the direction of propagation of the ultrasonic beam, pointing away from the transducer.
- **The lateral (La) axis:** within the image plane, perpendicular to the axial direction and pointing towards the left of the image.
- **The elevation (E) axis:** perpendicular to both the axial and the lateral directions, defined in such a way that the A–La–E coordinate system is right-handed. Thus, the elevation axis is defined perpendicular to the image plane.

This coordinate system is illustrated in Fig. 4.

Coordinate Transformations

When different coordinate systems exist, it is important to be able to transform measurements within one system to measurements made using another system. As will be further discussed in the next section, at present only the axial component of myocardial strain can be measured, that is, one component of strain as expressed in the ultrasound coordinate system (thus, the component along the scan line). However, in order to relate local strain to regional myocardial function, it is necessary to transform this component to the heart coordinate system.

In general, it is impossible to write closed-form mathematical expressions to describe this transformation since they depend on the echocardiographic view used and on the myocardial wall studied. However, when the ultrasonic beam is either parallel or perpendicular to the myocardial wall under investigation, this transformation becomes straightforward, since one component in one coordinate system corresponds directly to one component in the other system. For example, using the apical four-chamber view the ultrasound beam (and thus the image line) is normally parallel to the interventricular septum [Fig. 5(a)]. Thus, the axial strain component (in the ultrasound coordinate system) corresponds to the longitudinal component (in the heart coordinate system). Similarly, when the ultrasound beam is perpendicular to the posterior wall in a parasternal long-axis view, the axial component in one coordinate system corresponds to the radial component in the other [Fig. 5(b)].

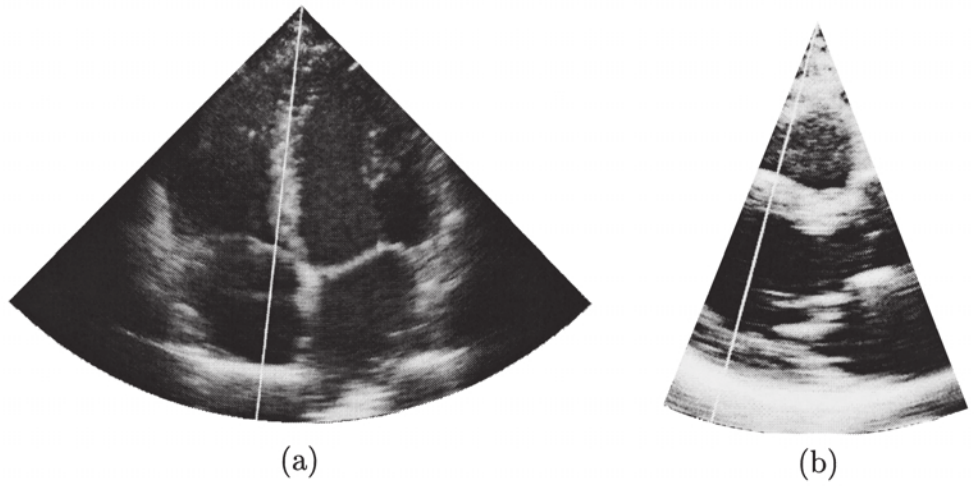

Figure 5. When the acquisition of the ultrasound data is done in such a way that an image line is parallel (a) or perpendicular (b) to the myocardial wall, coordinate transformation from the ultrasound coordinate system to the heart coordinate system becomes straightforward.

However, when the ultrasound beam impinges on the myocardial wall in an oblique way, the axial strain component corresponds to a combination of the radial, longitudinal and circumferential strains. This implies that in order to study regional myocardial deformation with current ultrasound techniques (only measuring the axial strain component), care has to be taken to acquire the appropriate data sets. For example, in a parasternal long-axis view, data sets must be acquired with the ultrasound beam perpendicular to the myocardium. Within the image plane, this can easily be verified visually. However, in the direction perpendicular to the image, the elevation direction, this is not always straightforward. In other words, when attempting to measure local strain, no oblique cross-sections of the ventricle should be acquired. Due to the motion of the heart during the cardiac cycle, this is often not possible. In such cases it should be kept in mind during any attempted analysis of the data that other strain components could have contributed to the measured axial strain.

Measurement of Cardiac Strain

Since the beginning of the 1980s, methods have been proposed to estimate strain by means of ultrasound[21–24]. Originally, most methods were developed for static organs such as the liver, breast, kidney or prostate. Part of these techniques deform these organs by means of an external force[25]. In these methods, stiffer tissues will deform less than more elastic tissues under the influence of an identical force. Thus, in this situation strain estimation can be directly related to the elastic properties of the tissue. For this reason, the technique has been termed 'elastography'. Note, however, that this passive compression need not be created by an external force but can be created by a force generated by the body itself: the intraluminal pulsing behaviour of the blood under arterial pressure can be used to deform artery walls which can then be imaged by intra-vascular ultrasound[26].

Recently, a series of ultrasound techniques have been developed to measure *myocardial* strain *in vivo*. Several different strain estimation techniques have been proposed based on the principles of elastography[27,28]. However, only one of them has successfully been applied for measuring myocardial strain[29]. The main difficulty in elastographic strain estimation of the heart is the fact that most myocardial segments exhibit a combination of relatively large motion and deformation. Additionally, this technique is highly computionally intensive, which makes its current application to 2D images in real-time impractical. Therefore, another approach based on Doppler myocardial imaging principles has been attempted[30]. Both techniques are briefly discussed in the subsequent paragraphs.

The Cross-Correlation Method

The properties of the received backscattered radio frequent signal from a distribution of scatterers (the local inhomogeneities in density and/or compressibility) are determined by the precise position of these scatterers: each scatterer will reflect the transmitted pulse as it is received; the received signal is the result of the interference between all these reflected wavelets. This implies that two different distributions of scatterers, D_A and D_B, will give rise to a different radio frequent signal pattern RF_A and RF_B, respectively.

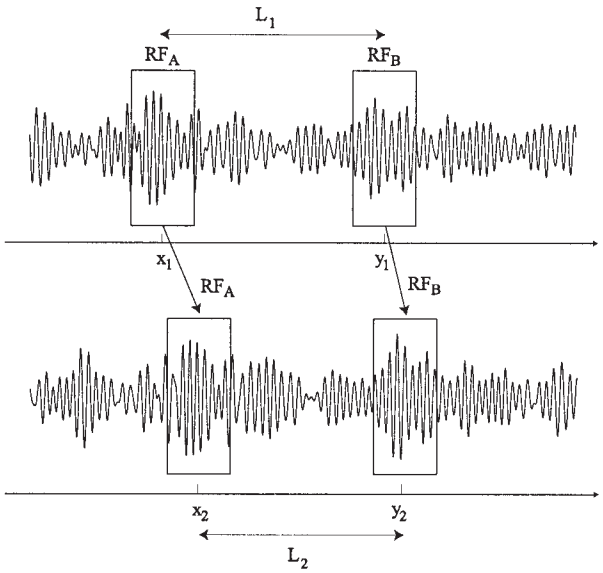

Figure 6. Schematic illustration of the fundamental concept of the cross-correlation method: a radio frequent signal line is acquired before and after deformation of the object; a local radio frequent signal pattern (resulting from a specific distribution of scatterers) is tracked between two subsequent acquisitions by means of the cross-correlation function, which is a measure for the similarity of two signals as a function of their relative phase.

Assume these distributions are located at different depths x_1 and y_1 along the same line of an ultrasonic image as illustrated in Figure 6. If the object containing the scatterer distributions D_A and D_B deforms in the *axial* direction, the two scattering regions will move relative to each other and as a consequence the corresponding radio frequent signal patterns RF_A and RF_B will move in the same manner. This is the fundamental concept behind the implementation of cross-correlation methodology: in this technique a radio frequent signal line is acquired before and after deformation of an object. A local radio frequent signal pattern (resulting from a specific distribution of scatterers) is then tracked between the two subsequent acquisitions by means of the cross-correlation function.

The cross-correlation function gives a measure of the similarity between two radio frequent signal patterns, such as RF_A and the second radio frequent signal, as a function of a relative time shift between the two. The time shift for which the cross-correlation function is maximal corresponds to the time shift for which both signals resemble most: that is, to the delay introduced

due to the motion of the radio frequent signal pattern. The change in distance between two specific radio frequent signal patterns RF_A and RF_B, which are L_1 and L_2 in Figure 6. respectively, can directly be used in equation (1) to estimate the local strain: it is the spatial gradient in the motion of the radio frequent signal patterns. Note that this technique can only determine the *axial* motion of the radio frequent signal patterns. As a result, only the axial strain component can be measured.

This method implies an assumption that the radio frequent signal pattern itself does not change between the two acquisitions. This assumption is only reasonable when the deformation of the object is relatively small (when the deformation of the object between the acquisition of the two radio frequent signals is small) and if there is not too much motion in the lateral and elevation directions. Thus, in order for this technique to work, acquisition of data at high temporal resolution is necessary.

For this reason, the cross-correlation method was initially implemented only for M-mode acquisition[29]. In this application the initial positions of the endo- and epicardium are manually indicated on the M-mode image by the user at a specific time point, end-diastole. The wall is then divided into a fixed number of layers. At all boundary layers the underlying radio frequent signal pattern is tracked as a function of time. Boundaries moving apart correspond to a positive strain value (compare to lengthening of a 1D bar). The result of radio frequent signal tracking is an estimation of the distance between two boundaries as a function of time: $L(t)$. This means that both Lagrangian and natural strain can be calculated.

The minimal strain that can be measured with this technique is (theoretically) the one corresponding to the motion of a fraction of the wavelength. In other words, a (theoretical) strain resolution in the order of micrometres can be achieved. Moreover, since the method is based on radio frequent signal tracking, no aliasing will occur since a specific radio frequent signal pattern can (theoretically) be tracked over any distance. Finally, since several layers are tracked, a transmural strain gradient can be measured.

The major disadvantage of this approach is that it is very computationally intensive. Although it has recently been implemented to measure strain in real-time[31], it is still limited to M-mode acquisition. As a consequence, the strain in only one region of myocardium can be investigated at a time. Such comparison of strain patterns in different myocardial regions (for the quantification of regional myocardial deformation) is a tedious and time-consuming task. This method has not yet been implemented in commercially available equipment.

The Velocity Gradient Method

Using the definitions in Figure 6, strain can be written as:

$$\varepsilon = \frac{L_2 - L_1}{L_1} = \frac{(y_2 - x_2) - (y_1 - x_1)}{y_1 - x_1} = \frac{(y_2 - y_1) - (x_2 - x_1)}{y_1 - x_1}, \quad (11)$$

where x_1, y_1 and x_2, y_2 are the positions of a specific radio frequent signal pattern before and after deformation, respectively. Dividing both sides of this equation by Δt, the time interval between the two acquisitions, gives:

$$\dot{\varepsilon} \approx \frac{\varepsilon}{\Delta t} = \frac{(y_2 - y_1)/\Delta t - (x_2 - x_1)/\Delta t}{y_1 - x_1} \approx \frac{v_2 - v_1}{L_1}. \quad (12)$$

In other words, *strain rate* can be expressed as the difference in velocities at both ends of an object of initial length L_1: it is the spatial gradient in velocities. Since local instantaneous myocardial velocities can be measured by colour Doppler, this means that strain rate information can be extracted from real-time, digitally stored myocardial data sets by post-processing. This principle was recognized from the beginning of Doppler myocardial imaging and resulted in a series of investigations into the radial transmural velocity gradient as an index of local contraction and relaxation[18,30,32–35]. All these studies made use of M-mode acquisition of velocity data sets and calculated the velocity gradient off-line by post-processing. Note, however, that Doppler myocardial imaging-techniques only estimate the *axial* component of the velocity vector, that is the component along the image line. As a consequence, only the *axial strain rate* can be calculated. It can be shown that the resulting strain rate curve is the *natural* strain rate (Appendix A). Thus, time-integrating this curve results in the *natural axial strain*. Since in this method strain rate is calculated based on the derived velocity data sets, aliasing can induce artifacts in the strain (rate) data (see later section for an example). Recently, real-time B-mode axial strain rate imaging has been implemented in a prototype clinical scanner[36].

The Relation Between Radial Strain Estimation and Grey-scale M-mode Data

The acquisition of grey-scale M-mode images at a high temporal and spatial resolution allows the definition of local myocardial thickening/thinning parameters[9]. In principle, the new ultrasound techniques described above can make the same measurements. The question then arises as to which extra benefits local strain imaging offers over conventional M-mode analysis. In summary, strain (rate) imaging has the following advantages over conventional M-mode data:

1. It allows the study of both regional radial thickening and thinning, and regional longitudinal and circumferential shortening and lengthening, and thus can measure three aspects of local function as opposed to only the radial parameters measured by traditional grey-scale M-mode.

2. It exploits the phase shift of the radio frequent signals rather than their amplitude, resulting in a better signal-to-clutter ratio (compare with Doppler techniques)[37].
3. Its calculation is based on the radio frequent signal rather than on its envelope. As a result, its spatial resolution is intrinsically better, as small displacements are more easily detected[38].
4. It does not require image segmentation to define the endo- and epicardial boundaries, and is thus less user-dependent and less time-consuming.

Note, however, that M-mode wall thickening/thinning measurements cannot directly be compared to strain measurements. Firstly, strain imaging measures the strain occurring within the sample volume (the local strain) while M-mode analysis determines the overall wall thickening/thinning (the global strain). The local and global strain values are not necessarily the same. Secondly, as explained above, strain imaging based on the velocity gradient methodology measures the natural strain while conventional wall thickening/thinning indices extracted from M-mode analysis correspond to the Lagrangian strain. Thus, in order to compare both measurements, equation (5) has to be used to convert one type of strain to the other one§.

The Current Status and Limitations of the Techniques

Practical Difficulties

As discussed above, two methods have been presented to calculate myocardial strain and strain rate data:

1. The cross-correlation method initially estimates regional motion from the radio frequent signal data. Strain is derived as a spatial gradient in motion. The strain rate can be obtained by calculating the temporal derivative of the strain curve.
2. The velocity gradient method calculates the strain rate curve as the spatial gradient in velocities. From this strain rate curve, the strain curve can be obtained by integration over time.

This is summarized in Figure 7. In other words, in order to obtain information on both the strain and the strain rate, both methods require the calculation of a (temporal or spatial) gradient and/or an integral. This causes two problems:

1. Calculating gradients numerically (i.e. with a digital computer) is very sensitive to noise, as illustrated in Figure 8, where a signal without and with noise [Fig. 8(a) and (c)] is shown together with its numerically calculated derivative [Fig. 8(b) and (d)]. Note that the noise level in Fig. 8(c) was very small. As a consequence, the motion or velocity data sets (depending on which method is used) have to be smoothed in order to obtain strain or strain rate curves, respectively, which are not too noisy. This can be done by measuring the average motion or velocity value for a region around each pixel within the image. Additionally, smoothing of the extracted strain (rate) data can be performed to improve the resulting strain (rate) image. As a result, the spatial resolution of these techniques becomes relatively poor. Typical spatial resolution values for the cross-correlation and the velocity gradient method are 1–3 mm and 2–5 mm, respectively. This means that no two independent measurements can be made accurately for points closer than these values apart. As a consequence, studying local intramural gradients in strain rate or strain might not be possible with the velocity gradient methodology.
2. In order to calculate regional strain in the velocity gradient methodology, the strain rate curves are time-integrated. However, time integrating the strain rate curve can result in a drifting of the strain curve [as illustrated in Fig. 9(a)]. The main factors which can induce this drifting are: a poor frame rate (such as peak values missing), a bias in the strain rate estimate (for example, the strain rate is systematically estimated too high), an inhomogeneous strain distribution within the sample volume or angle changes during the cardiac cycle. However, we know that at the end of the cardiac cycle strain should be zero, as the heart muscle returns to its initial shape after a complete heart cycle: there cannot be a net strain. Thus, using this boundary condition and assuming that the error introduced is not dependent on the

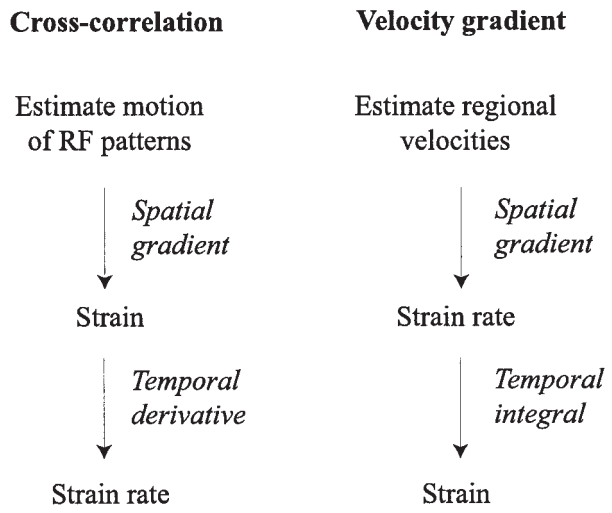

Figure 7. Schematic overview of the operations required for strain and strain rate estimation in the cross-correlation and the velocity gradient methodologies.

§In fact, this conversion formula only holds when the deformation rate is constant as a function of time. Since this assumption is not valid for the heart, this equation can only be used as a first approximation.

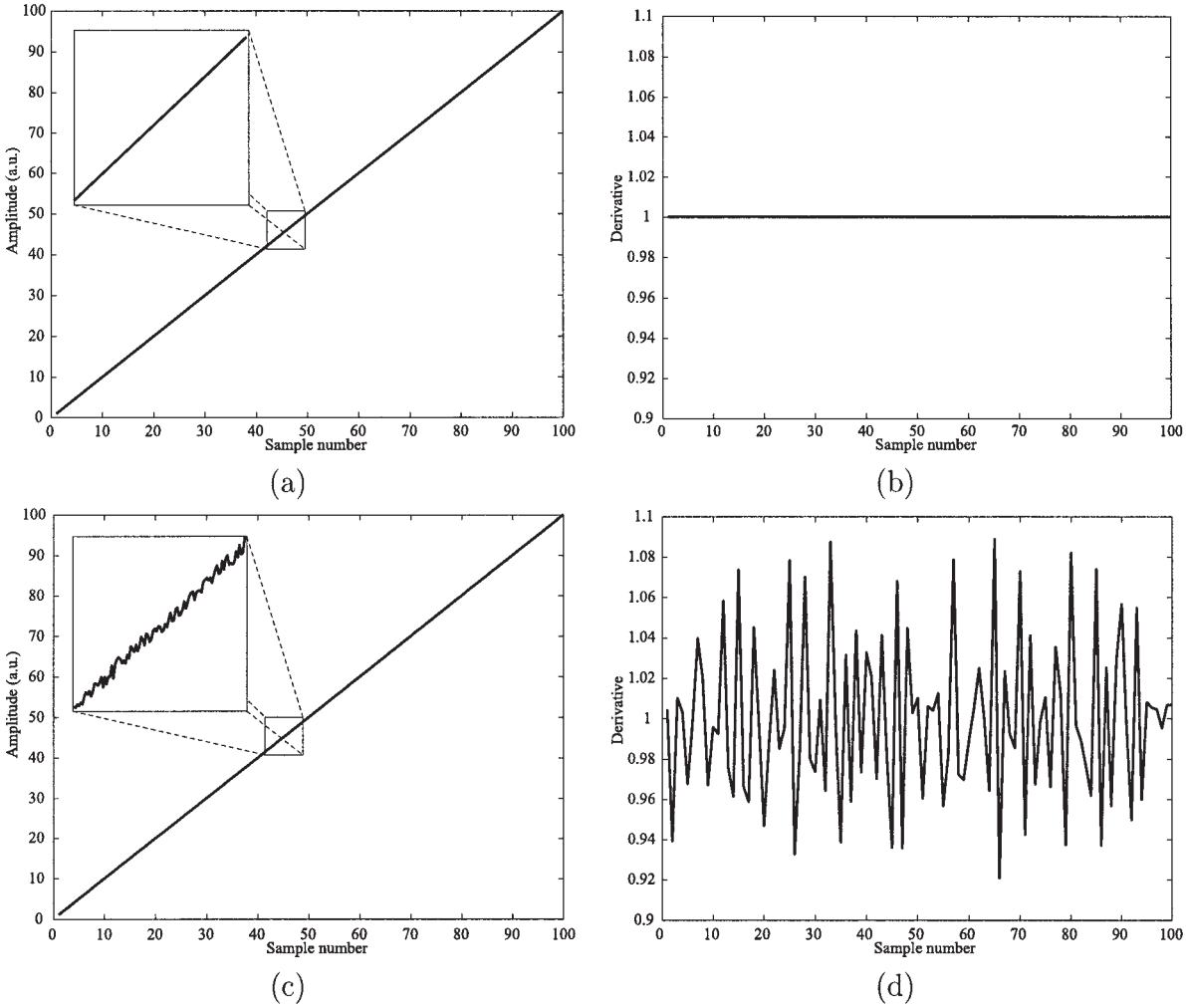

Figure 8. Illustration of the sensitivity of the numerical derivation to noise: a (perfect) straight line (a) results in a precise definition of the derivative (b). However, adding a small amount of (measurement) noise to this line (c) results in a very noisy numerical derivative (d).

amplitude of the strain rate nor on the position within the heart cycle, this drifting can automatically be compensated for [Fig. 9(b)].

Angle Dependency of Strain Measurements

One of the major criticisms of velocity, strain rate and strain imaging has been that these techniques are angle-dependent, since only the axial component of the true 3D velocity vector or deformation is measured. As already discussed above, this problem can be partially avoided by making sure that insonation is either perpendicular or parallel to the myocardial wall during acquisition of the data sets. Moreover, if some simple assumptions are made about the way the heart deforms, the strain rate error induced due to imaging the heart wall under an angle can be estimated[39]. This means that the angle dependency of the strain (rate) technique can be compensate for. Note however that, although the amplitude of the velocity, strain rate or strain curves can be influenced by the insonation angle, in clinical practice this angle dependency does probably not have an important influence on the timing of specific events nor on the profiles of the curves. However, the importance of the influence of the angle dependency needs to be investigated further.

Only a Limited Number of Strain Components can be Measured

Since only the axial strain component can be measured with the current cardiac ultrasound strain estimation techniques, and since the heart can only be visualized in a limited number of views, not all strain components (radial, longitudinal and circumferential) can be measured for all myocardial segments. In general, longitudinal strain can be measured in all left ventricular segments using the apical two-, three- or four-chamber

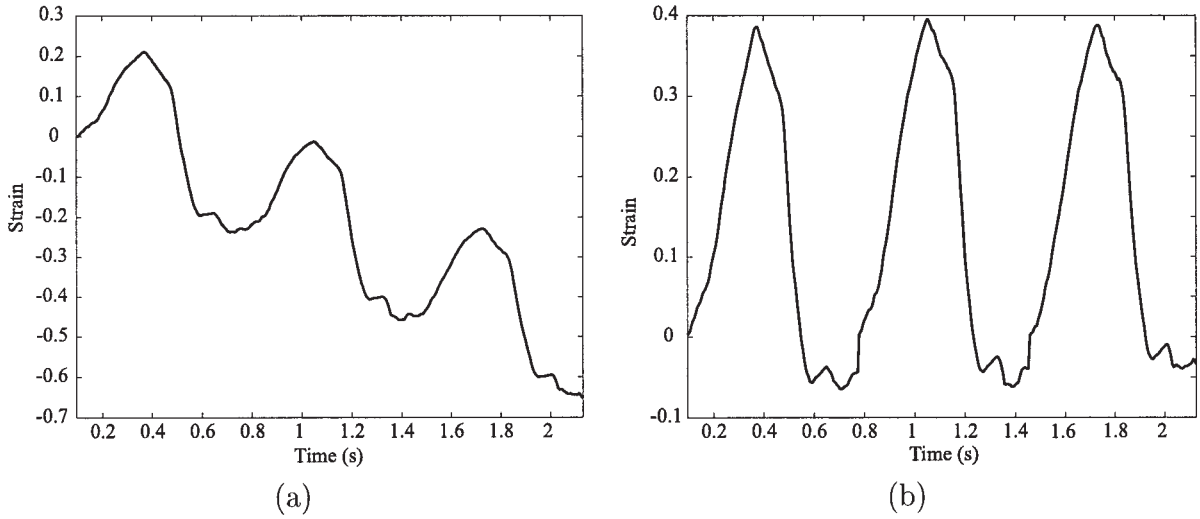

Figure 9. (a) Time-integrating the strain rate curve can result in a drifting of the strain curve. However, using the physical boundary condition that the strain value at the end of the cardiac cycle should be zero (b), this effect can automatically be compensated for.

views. However, radial and circumferential strain can only be assessed in some segments, for example, radial strain in the posterior wall or circumferential strain in the lateral wall using a parasternal short-axis view.

Clinical Examples

The clinical examples shown in this section to illustrate the potential role of these new modalities are all based on the velocity gradient method. Figure 10 (a) shows one frame of the original colour Doppler B-mode acquisition in an apical four-chamber view from a normal volunteer. From the digitally stored data sets, velocity profiles over one cardiac cycle, that is one R–R interval, are extracted for an apical, mid and basal segment of the intra-ventricular septum. The timing of aortic valve closure and mitral valve opening is indicated by a vertical dashed line. The motion during systole, early- and atrial filling (the S, E and A wave) can clearly be identified. Moreover, a clear base to apex gradient in velocities can be recognized with velocities being higher in the basal segments of the myocardium. Time-integrating the velocity curve results in the displacement curve shown in the right of Figure 10. As expected in the apical view, there is motion towards the transducer during systole and away from the transducer during diastole. Moreover, the maximal displacement of the apical segments is smaller than that of the basal ones.

Regionally calculating the local spatial gradient in myocardial velocities results in an estimate of the local strain rate as explained above. The strain rate image extracted from the same velocity colour Doppler data set is shown in Fig. 10(b). Again, the strain rate curves are extracted from the apical, mid and basal segments of the septum and the timing of aortic valve closure and mitral valve opening is indicated. During systole a negative strain rate value is measured, indicating regional longitudinal shortening of the ventricle, while the biphasic relaxation of the wall (rapid filling and filling with atrial contraction) can also be identified based on the two lengthening phases — positive strain rate phases. Time integration of the strain rate curves results in the regional strain curves: it can be seen that the wall shortens during systole and lengthens during diastole.

In order to investigate the velocity or strain rate profiles of several segments within the myocardial wall simultaneously, a curved M-mode image can be constructed[40]. Therefore, the velocity or strain rate information of all points along a manually indicated curved line within the image is colour-coded and shown as a function of time. A curved velocity and strain rate M-mode image from a normal volunteer is shown in Figure 11: the vertical axis indicates different points in the septum while the horizontal axis represents time. The synchronous nature of the velocity and strain rate changes throughout the septal wall can be appreciated.

Figure 10 (opposite). Colour Doppler B-mode acquisition of a normal volunteer (a) together with its derived strain rate image (b). At specific points within the interventricular septum time profiles of the velocity (a) and strain rate (b) were extracted over one cardiac cycle (middle). Time integrating these curves results in the displacement and strain curves, respectively (right). The vertical dashed lines indicate the position of aortic valve closure (AVC) and mitral valve opening (MVO).

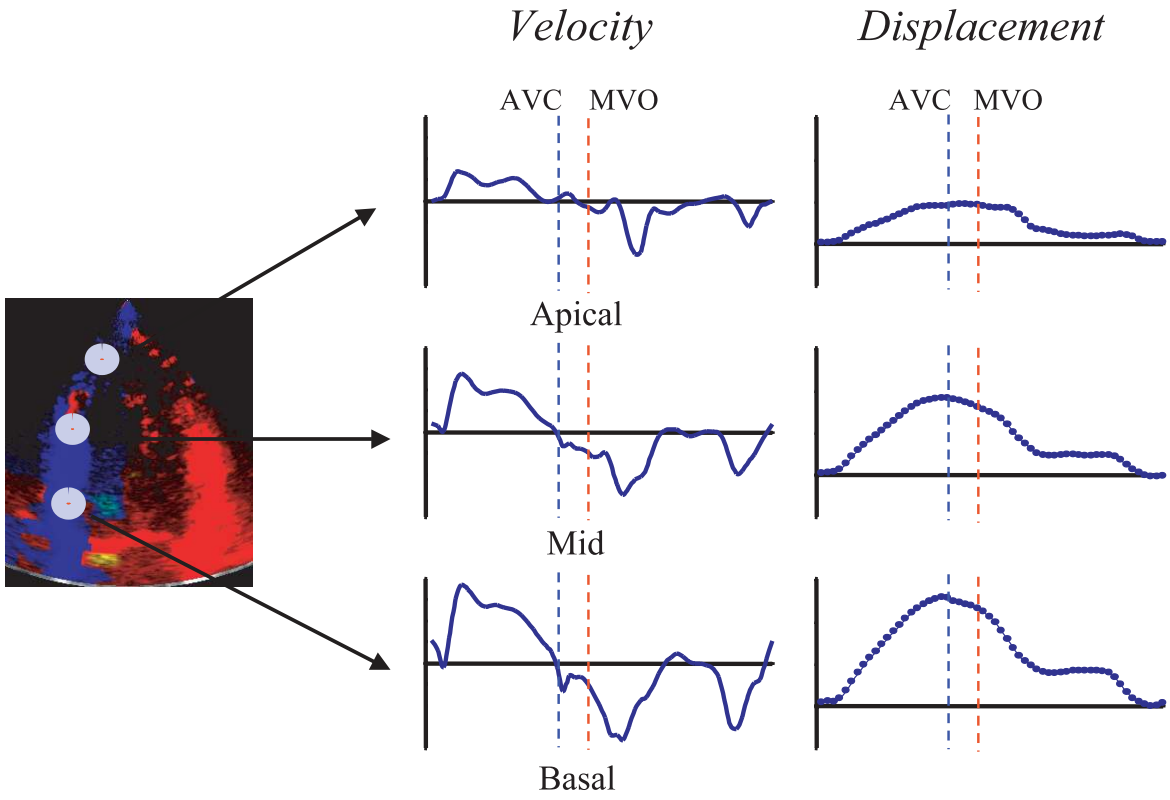
Velocity
Displacement
AVC
MVO
AVC
MVO
Apical
Mid
Basal

(a)

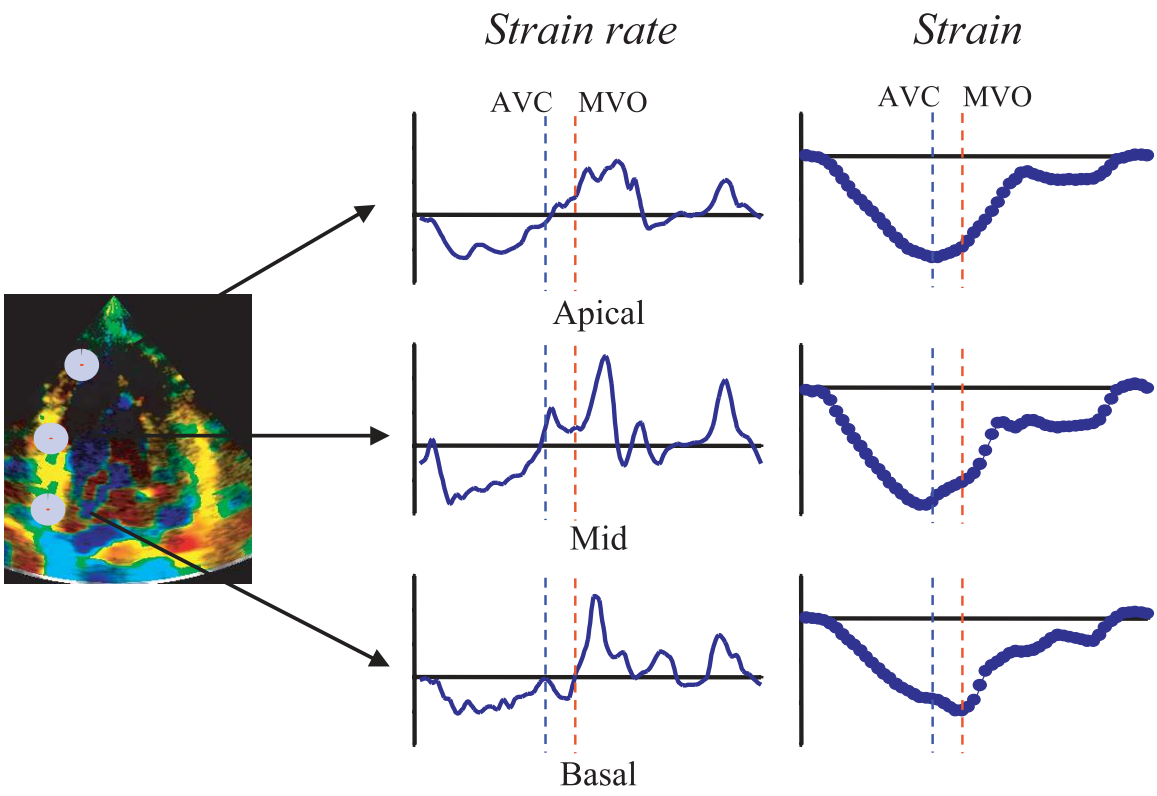
Strain rate
Strain
AVC
MVO
AVC
MVO
Apical
Mid
Basal

(b)

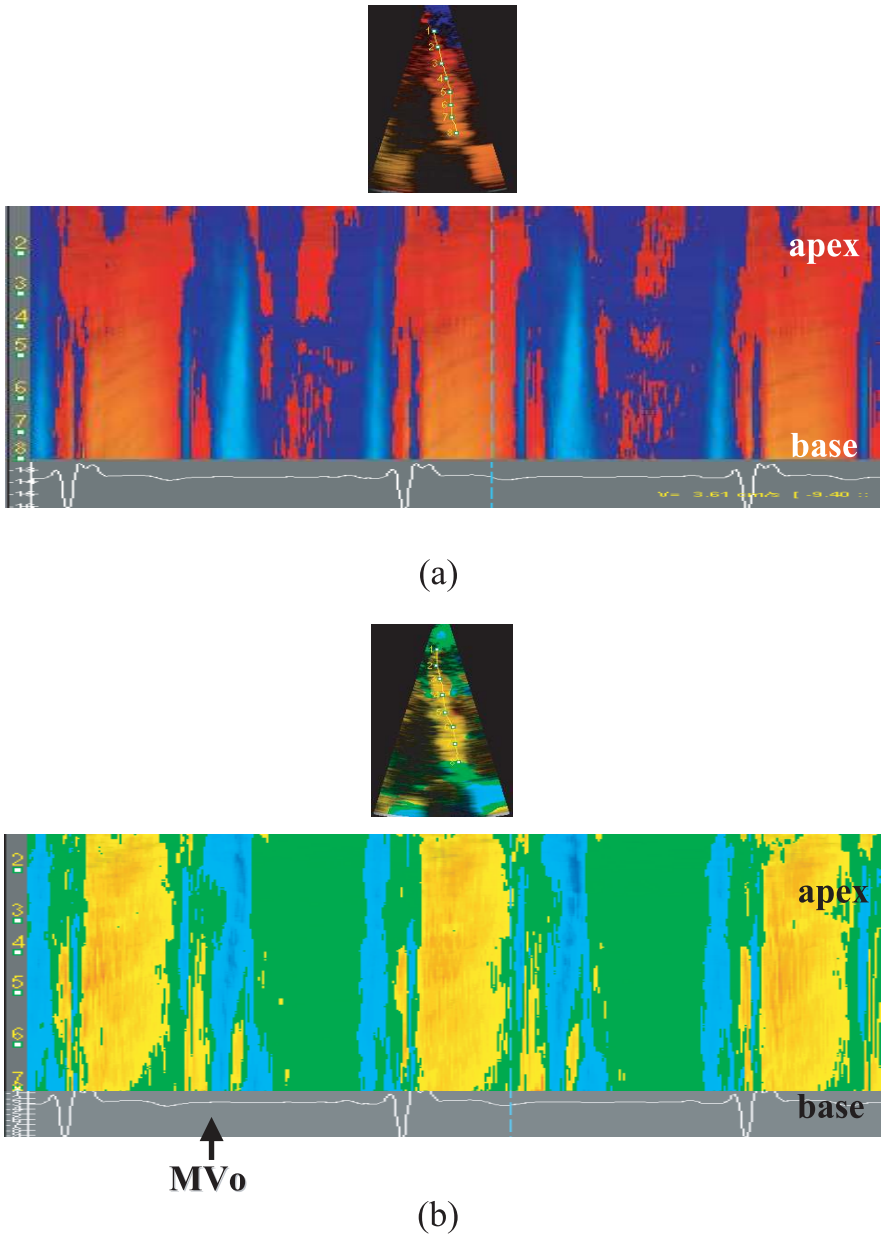

Figure 11. Example of a curved M-mode velocity (a) and strain rate (b) image of a normal volunteer: the velocity or strain rate information of all points along a manually indicated curve on the image, is colour coded and shown as a function of time.

Again, the systolic, early and atrial filling phases can be identified. Note that the velocity base to apex gradient can also be seen on the curved M-mode image.

In a patient with severe lateral wall ischaemia the same images can be extracted, as shown in Figure 12. The velocity image does not accurately characterize the different contractile state of the lateral wall since global motion and/or rotation of the heart can induce the measured velocities. However, the strain rate image clearly demonstrates that the overall rate of deformation (and thus the total deformation) of the ischaemic lateral wall is much lower.

Finally, Figure 13 gives an example of an aliased strain rate data set. Aliasing can be identified within a strain rate image by artifacts which appear at the boundaries of the clipped velocity estimates. The effect can be observed both in the 2D strain rate image and in the individual strain rate curves. It is the results of calculating strain rate as the spatial gradient in velocities. Note that aliasing can be compensated for by means of, for example, phase unwrapping techniques, and thus is not a fundamental problem of the methodology. Moreover, when the cross-correlation methodology is used aliasing would not occur at all,

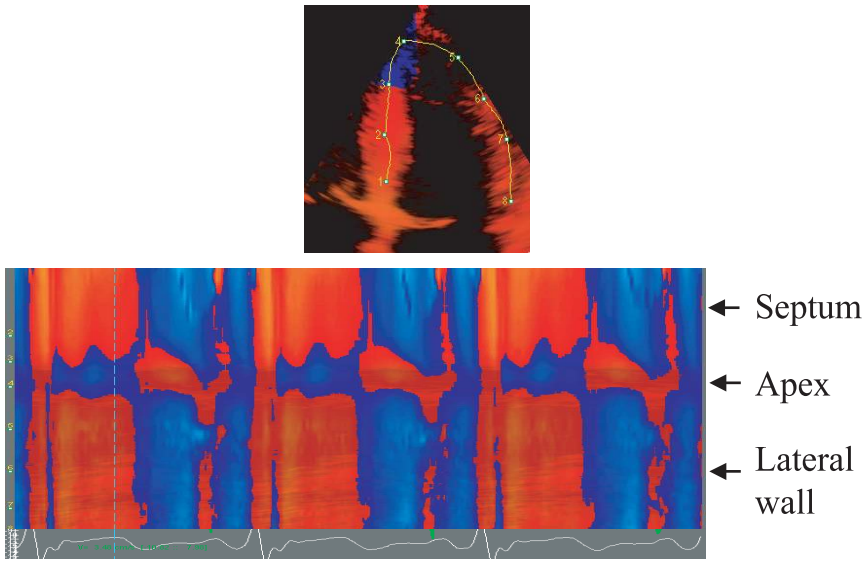

(a)

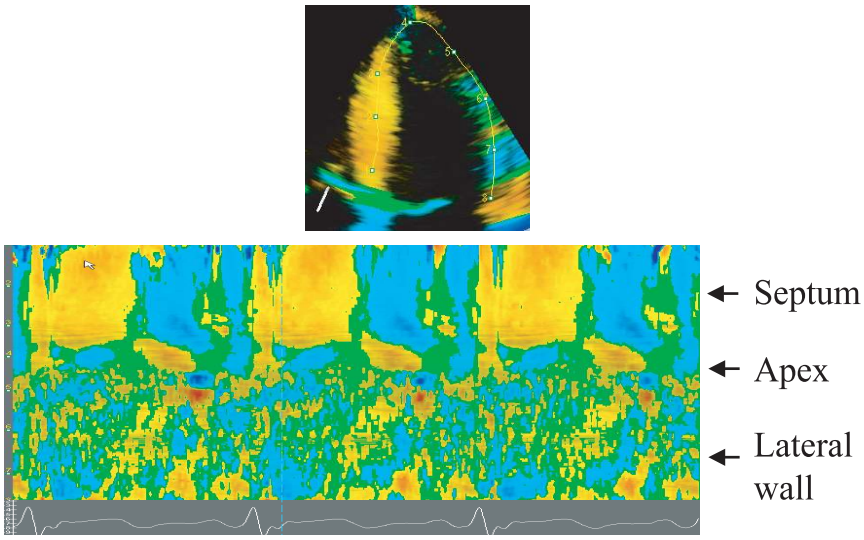

(b)

Figure 12. Example of a curved M-mode velocity (a) and strain rate (b) image of a patient with severe lateral wall ischaemia. The abnormal strain rate profile within this wall is obvious. However, the velocity information does not resolve the abnormal regional function.

since a specific radio frequent signal pattern can (theoretically) be tracked over any distance.

Conclusions

Strain rate and strain imaging are potentially important new tools for the quantification of regional myocardial function. Initial *in vitro* and *in vivo* studies have shown promising results. However, the clinical relevance of the technique remains to be proven. The introduction of these imaging modalities into clinical practice will require the definition of normal segmental values for strain and strain rate (both in the radial, longitudinal and circumferential direction). At the time of writing these values are not available. As far as pitfalls are concerned, the problem of angle dependency has probably been overestimated, since in a clinical situation timing of regional myocardial events can be represented accurately. Moreover, compensation for this angle dependency seems possible. A more fundamental problem of

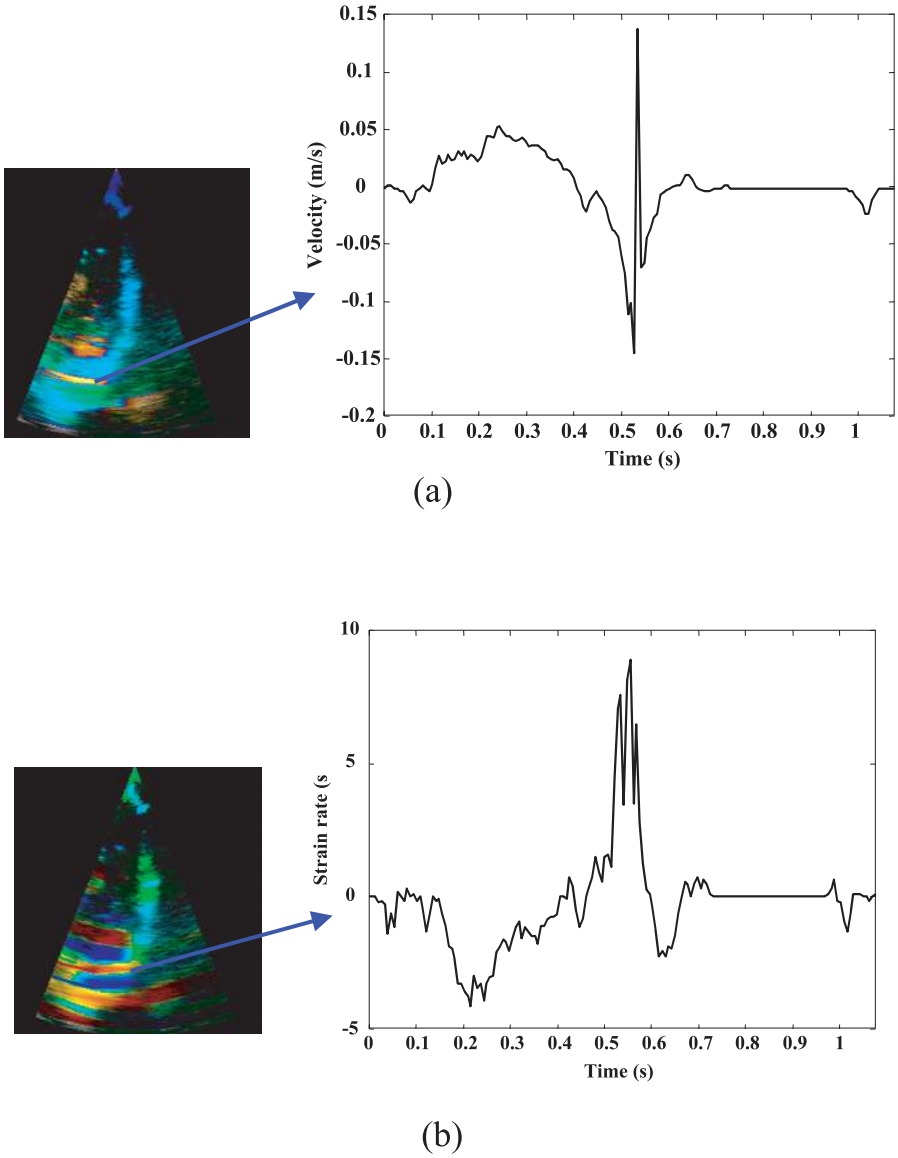

Figure 13. Example of an aliased colour Doppler data set (a) and the resulting strain rate artifact (b). The strain rate artifact represents itself by the extremely high strain rate estimates. It can be seen both in the 2D strain rate image (left) and in the extracted strain rate profiles (right).

the technique is that currently for a myocardial segment only one of the possible nine strain components can be measured (unless two different acquisitions are made from different echocardiographic views, in which case two components can be assessed). It must therefore be determined whether such a uni-dimensional data set can sufficiently describe the clinical substrate being investigated. Further attempts will have to be made to estimate the other myocardial strain (rate) components by ultrasound as well. This again is theoretically feasible by using information of adjacent scan lines and/or by applying the principles of conservation of mass[39]. Moreover, shear strain estimation has been developed in elastography and should thus, theoretically, also be feasible for cardiac strain[41].

References

[1] Gibson DG, Prewitt TA, Brown DJ. Analysis of left ventricular wall movement during isovolumic relaxation and its relation to coronary artery disease. *Br Heart J* 1976; **38:** 1010–1019.

[2] Lang RM, Vigon P, Weinert L, Bednarz J, Korcarz C, Sandelski J, Koch R, Prater D, Mor-Avi V. Echocardiographic quantification of regional left ventricular wall motion with color kinesis. *Circulation* 1996; **93:** 1877–1885.

[3] Heger JJ, Weyman AE, Wann LS, Dillon JC, Feigenbaum H. Cross-sectional echocardiography in acute myocardial infarction: detection and localization of regional left ventricular asynergy. *Circulation* 1979; **60:** 531–538.

[4] Cwaijg E, Cwajg J, He ZX, Hwang WS, Keng F, Nagueh SF, Verani MS. Gated myocardial perfusion tomography for the assessment of left ventricular function and volumes:

comparison with echocardiography. *J Nucl Med* 1999; **40:** 1857–1865.

[5] Beyar R, Shapiro EP, Graves WL, Rogers WJ, Guier WH, Carey RL, Soulen EA, Zerhouni ML, Weisfeldt ML, Weiss JL. Quantification and validation of left ventricular wall thickening by a three-dimensional volume element magnetic resonance imaging approach. *Circulation* 1990; **81:** 297–307.

[6] Rademakers FE, Bogaert J. Left ventricular myocardial tagging. *Int J Card Imaging* 1997; **13:** 233–245.

[7] Schermund A, Gerber T, Behrenbeck T, Reed JE, Sheedy PF, Christian TF, Rumberger JA. Measurement of myocardial infarct size by electron beam computed tomography: a comparison with 99mtc sestamibi. *Invest Radiol* 1998; **33:** 313–321.

[8] Shen MY, Liu YH, Sinusas AJ, Fetterman R, Bruni W, Drozhinin OE, Zaret BL, Wackers FJ. Quantification of regional myocardial wall thickening on electrocardiogram-gated spect imaging. *J Nucl Cardiol* 1999; **6:** 583–595.

[9] Guth B, Savage R, White F, Hagan A, Samtoy L, Bloor C. Detection of ischemic wall dysfunction: comparison between m-mode echocardiography and sonomicrometry. *Am Heart J* 1984; **107:** 449–457.

[10] McDicken WM, Sutherland GR, Moran CM, Gordon LN. Colour doppler velocity imaging of the myocardium. *Ultrasound Med Biol* 1992; **18:** 651–654.

[11] Sutherland GR, Stewart MJ, Groundstroem WE, Moran CM, Fleming A, Guell-Peris FJ, Riemersma RA, Fenn LN, Fox KAA, McDicken WN. Color doppler myocardial imaging: a new technique for the assessment of myocardial function. *J Am Soc Echocardio* 1994; **7:** 441–458.

[12] Garcia MJ, Rodriguez L, Ares M, Griffin BP, Thomas JD, Klein AL. Differentiation of constrictive pericarditis from restrictive cardiomyopathy: assessment of left ventricular diastolic velocities in longitudinal axis by doppler tissue imaging. *J Am Coll Cardiol* 1996; **27:** 108–114.

[13] Katz WE, Gulati VK, Mahler CM, Gorcsan J, III. Quantitative evaluation of the segmental left ventricular response to dobutamine stress by tissue doppler echocardiography. *Am J Cardiol* 1997; **79:** 1036–1042.

[14] Severino S, Caso P, Galderisi M, De Simone L, Petrocelli A, de Divitiis O, Mininni N. Use of pulsed doppler tissue imaging to assess regional left ventricular diastolic dysfunction in hypertrophic cardiomyopathy. *Am J Cardiol* 1998; **82:** 1394–1398.

[15] Mankad S, Murali S, Kormos RL, Mandarino WA, Gorcsan J, III. Evaluation of the potential role of color-coded tissue doppler echocardiography in the detection of allograft rejection in heart transplant recipients. *Am Heart J* 1999; **138:** 721–730.

[16] Pasquet A, Armstrong G, Beachler MS, Lauer L, Marwick TH. Use of segmental tissue doppler velocity to quantitate exercise echocardiography. *J Am Soc Echocardio* 1999; **12:** 901–912.

[17] Jamal F, Derumeaux G, Douillet R, Roussel C, Cribier A. Analyse et quantification de la contraction longitudinale ventriculaire gauche dans l'infarctus du myocarde: apport du doppler tissulaire myocardique. *Arch Maladies Coeur Vaisseaux* 1999; **92:** 315–322.

[18] Tsutsui H, Uematsu M, Shimizu H, Yamagishi M, Tanaka N, Matsuda H, Miyatake K. Comparative usefulness of myocardial velocity gradient in detecting ischemic myocardium by a dobutamine challenge. *J Am Coll Cardiol* 1998; **31:** 89–93.

[19] Mirsky I, Ghista DN, Sandler H. *Cardiac Mechanics: Physiological Clinical, and Mathematical Considerations.* 1974; New York: John Wiley & Sons Inc.

[20] D'hooge J, Jamal F, Kukulski T, Kowalski M, Heimdal A, Thoen J, Suetens P, Rademakers FE, Bijnens B, Sutherland GR. Calculation of strain values from strain rate curves: how should this be done? *Eur Heart J* 2000 **21**(Suppl.): 335.

[21] Dickinson RJ, Hill CR. Measurement of soft tissue motion using correlation between a-scans. *Ultrasound Med Biol* 1982; **8:** 263–271.

[22] Wilson LS, Robinson DE. Ultrasonic measurement of small displacements and deformations of tissue. *Ultrasonic Imaging* 1982; **4:** 71–82.

[23] Meunier J, Bertrand M, Mailloux GE, Petitclerc R. Local myocardial deformation computed from speckle motion. *Proceedings of IEEE Computers in Cardiology* 1989; 133–136.

[24] Parker KJ, Huang SR, Musulin RA, Lerner RM. Tissue response to mechanical vibrations for sonoelasticity imaging. *Ultrasound Med Biol* 1990; **16:** 241–246.

[25] Ophir J, Cespedes I, Ponnekanti H, Yazdi Y, Li X. Elastography: a method for imaging the elasticity in biological tissues. *Ultrasonic Imaging* 1991; **13:** 111–134.

[26] de Korte CL, Carlier SG, Mastik F, van der Steen AFW, Cespedes I, Bom N. Intravascular ultrasound elastography: preliminary clinical experience (abstract). *Circulation* 1999; **100:** (Suppl I), I229.

[27] Hein IA, O'Brien WD. Current time domain methods for assessing tissue motion by analysis from reflected ultrasound echoes — a review. *IEEE Trans Ultrasonics, Ferro-electrics Freq Control* 1993; **40:** 84–102.

[28] Gao L, Parker KJ, Lerner RM, Levenson SF. Imaging of the elastic properties of tissue — a review. *Ultrasound Med Biol* 1996; **22:** 959–977.

[29] Kanai H, Hasegawa H, Chubachi N, Koiwa Y, Tanaka M. Noninvasive evaluation of local myocardial thickening and its color-coded imaging. *IEEE Trans Ultrasonics, Ferro-electrics Freq Control* 1997; **44:** 752–768.

[30] Fleming D, Xia X, McDicken WN, Sutherland GR, Fenn L. Myocardial velocity gradients detected by doppler imaging. *Br J Radiol* 1994; **67:** 679–688.

[31] Kanai H, Koiwa Y, Zhang J. Real-time measurements of local myocardium motion and arterial wall thickening. *IEEE Trans Ultrasonics, Ferro-electrics Freq Control* 1999; **46:** 1229–1241.

[32] Uematsu M, Miyatake K, Tanaka N, Matsuda H, Sano A, Yamazaki N, Hirama M, Yamagishi M. Myocardial velocity gradient as a new indicator of regional left ventricular contraction: detection by a two-dimensional tissue doppler imaging technique. *J Am Coll Cardiol* 1995; **26:** 217–223.

[33] Palka P, Lange A, Fleming AD, Donnelly JE, Dutka DP, Starkey IR, Shaw TRD, Sutherland GR, Fox KAA. Differences in myocardial velocity gradient measured throughout the cardiac cycle in patients with hypertrophic cardiomyopathy, athletes and patients with left ventricular hypertrophy due to hypertension. *J Am Coll Cardiol* 1997; **30:** 760–768.

[34] Derumeaux G, Ovize M, Loufoua J, Pontier G, Andr Fouet X, Cribier A. Assessment of nonuniformity of transmural myocardial velocities by color-coded issue doppler imaging. *Circulation* 2000; **101:** 1390–1395.

[35] Palka P, Lange A, Ferrington C, Fox KAA. Mean myocardial velocity mapping in quantifying regional myocardial contractile reserve in patients with impaired left ventricular systolic function: Doppler myocardial imaging study. *J Am Soc Echocardio* 2000: **12:** 96–107.

[36] Heimdal A, Stoylen A, Torp H, Skjaerpe T. Real-time strain rate imaging of the left ventricle by ultrasound. *J Am Soc Echocardio* 1998; **11:** 1013–1019.

[37] Sutherland GR, Bijnens B, McDicken WN. Tissue doppler echocardiography: historical perspectives and technological considerations. *Echocardiography* 1999; **16:** 445–453.

[38] Alam SK, Ophir J. On the use of envelope and rf signal decorrelation as tissue strain estimators. *Ultrasound Med Biol* 1997; **23:** 1427–1433.

[39] Heimdal A. *Doppler Based Ultrasound Imaging Methods for Noninvasive Assessment of Tissue Viability.* PhD thesis, Norwegian University of Science and Technology, Norway, 1999.

[40] Broden LA, van der Linden J, Olstad B. Echocardiographic functional images based on tissue velocity information. *Herz* 1998; **23:** 491–498.

[41] Konofagou EE, Ophir J. A new method for estimation and imaging of lateral strains and poisson's ratios in tissues. *Ultrasound Med Biol* 1998; **24:** 1183–1199.

Appendix A

Take a 1D bar with end-points A and B. Assume that at time instance t these points have an instantaneous coordinate $r_A(t)$ and $r_B(t)$, respectively, and that they are moving with the instantaneous velocities $v_A(t)$ and $v_B(t)$ (Fig. 14). If we assume *linear*, *uniform strain* within the bar, the instantaneous velocity of an arbitrary point within the bar, having a coordinate r, can be written as:

$$v(r,t) = v_A(t) + \frac{v_B(t) - v_A(t)}{L(t)} . (r(t) - r_A(t)), \qquad (13)$$

with $L(t) \equiv r_B(t) - r_A(t)$ the instantaneous length of the bar. Note that the proportionality factor $v_B(t) - v_A(t)/L(t)$ is in fact the true strain rate of the bar.

Assume that a sample volume with a fixed length L_S and end-points having coordinates r_1 and r_2, respectively, is put inside this (deforming) bar. By using equation (13), this implies that the measured instantaneous strain rate $\dot{\varepsilon}(t)$ is given by:

$$\begin{aligned}\dot{\varepsilon}(t) &= \frac{v(r_2,t) - v(r_1,t)}{r_2 - r_1} \\ &= \frac{\left(v_A(t) + \frac{v_B(t) - v_A(t)}{L(t)} . (r_2 - r_A(t))\right) - \left(v_A(t) + \frac{v_B(t) - v_A(t)}{L(t)} . (r_1 - r_A(t))\right)}{r_2 - r_1} \\ &= \frac{\frac{v_B(t) - v_A(t)}{L(t)} . (r_2 - r_1)}{r_2 - r_1} \\ &= \frac{v_B(t) - v_A(t)}{L(t)},\end{aligned}$$

which is the true instantaneous strain rate. Since the denominator of this expression takes into account the instantaneous length of the bar, $L(t)$ rather than its initial length $L(t_0) \equiv L_0$, this implies that the *natural* strain rate is measured. Note, however, that this is only true if the assumption of linear, uniform strain within the bar holds.

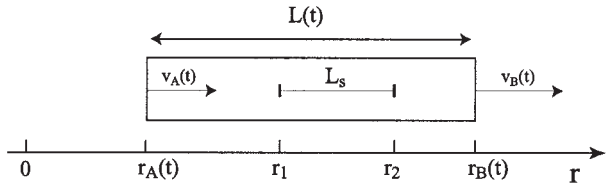

Figure 14. Geometry used to derive a relation showing that the velocity gradient methodology in fact measures the natural strain rate.